- Supporting Information -

Origin of Axial and Radial Expansions in Carbon Nanotubes Revealed by Ultrafast Diffraction and Spectroscopy

Giovanni M. Vanacore, Renske M. van der Veen†, and Ahmed H. Zewail*

Affiliations:

Physical Biology Center for Ultrafast Science and Technology, Arthur Amos Noyes Laboratory of Chemical Physics, California Institute of Technology, Pasadena, CA 91125, USA

†Present address: Max Planck Institute for Biophysical Chemistry, Göttingen (Germany), and the Deutsches Elektronen Synchrotron (DESY), Hamburg (Germany).

*To whom correspondence should be addressed. E-mail: zewail@caltech.edu

S.1 Raman spectral characterization and additional diffraction data

The Raman spectral characterization of the investigated carbon nanotubes was performed with a Renishaw Raman microprobe at ambient conditions, using backscattering configuration and laser excitation of 514.3 nm.

The Raman spectrum in Figure S1 for multi-walled nanotubes, which were grown by Chemical Vapor Deposition (CVD – Aldrich, > 90 % purity), reveals their typical signature. The strong peaks at 1349 cm^{-1}, 1582 cm^{-1}, 2697 cm^{-1}, and 2935 cm^{-1} correspond to the D, G, 2D and D+G bands, respectively.[1] The G band has E_{2g} symmetry and arises from in-plane bond stretching of pairs of sp^2 carbon atoms. The D band is a symmetrical stretch with A_{1g} symmetry. It is forbidden in perfect graphite, but becomes active in presence of structural defects. The 2D and D+G modes are the overtones of the D and G bands, as evident from the values of their frequencies: ~ 2×1349 cm^{-1} and ~ 1582+1349 cm^{-1}, respectively.

When Figure S1 is compared to the Raman spectra commonly reported in the literature for CVD-grown multi-walled nanotubes,[2,3,4,5] a good quantitative agreement is obtained. In this case, the ratio of the intensity of the D and G bands (I_D/I_G), which is often used as a measure of disorder, varies in the range of 0.47 – 1.2. In our case, we have $I_D/I_G = 0.86$. Moreover, the full width at half maximum (FWHM) values commonly reported for the G and D bands are in the range of 55 – 80 cm^{-1},[2-5] and well compare with the value of ~ 70 cm^{-1} observed here. Hence, the multi-walled carbon nanotubes investigated in the present study are fully in accord with the expected structures.

For the “single-walled” nanotubes, the Raman spectrum is shown in Figure S2. The G band consists of two main components at 1596 cm^{-1} (G^+) and 1574 cm^{-1} (G^-). The G^+ peak is associated with longitudinal optical phonons (LO) along the tube axis, whereas the G^- peak is

associated with transverse optical phonons (TO) along the circumferential direction.[1] Their Lorentzian lineshapes, their frequency values, and the FWHM of ~ 12 cm^{-1} are consistent with a semiconducting character of the single-walled tubes.[1,6] A very low amount of disorder is evident from the weak D band at 1345 cm^{-1} ($I_D/I_{G^+} = 0.04$).

To ensure that no radiation damage has occurred during the measurements, we monitored the intensity of the (002) and (110) diffraction peaks at zero time-delay as a function of the acquisition time (see Figure S3). No detectable change is observed in both cases, attesting that the same degree of crystallinity is preserved during the measurements made here.

The experimental time dependence of the peak-position change shown in Figures 2 and 3 for the radial (002) and the axial (110) reflections was similarly obtained for the (004) and (100) peaks, shown in Figure S4. For the (004) reflection, we found a single time constant of 4.5 ± 0.75 ps. For the (100) reflection, we determine a time constant of 1.7 ± 0.5 ps for the initial change and of 12 ± 3 ps for the final recovery.

S.2 Equilibrium heating model

According to the equilibrium heating model[7] the temperature increase, ΔT, induced by the laser irradiation can be calculated from:

$$f = \int_{T_0}^{T_0+\Delta T} C_p(T)dT \qquad (1)$$

where f is the absorbed fluence, $T_0 = 300$ K is the initial temperature, and $C_p(T)$ is the temperature-dependent heat capacity.[8] The absorbed fluence is given by:

$$f = f_0 \frac{1-R}{\xi} \qquad (2)$$

where f_0 is the incident fluence, $R = 0.1$ is the reflectivity[9] and $\xi = 133$ nm is the penetration depth[10] at $\lambda = 800$ nm for turbostratic graphitic materials. The thermal motions for a given temperature increase, ΔT, induce a loss of interference that results in a reduction of the diffraction intensity, quantitatively described by the Debye-Waller relation:

$$\ln\left(\frac{I_0}{I}\right) = 2[W(T, \Theta_D) - W(T_0, \Theta_D)] \quad (3)$$

where $T = T_0 + \Delta T$, Θ_D is the Debye temperature, W is the Debye-Waller factor, and I_0 and I are the diffraction intensities before and after the optical excitation, respectively. The Debye-Waller factor that can be expressed as:

$$W(T, \Theta_D) = \frac{3\hbar^2 s^2}{2MK_B\Theta_D}\left[\frac{1}{4} + \left(\frac{T}{\Theta_D}\right)^2 \int_0^{\Theta_D/T} \frac{\mu}{\exp(\mu) - 1} d\mu\right] \quad (4)$$

where M is the atomic mass of the carbon atoms, K_B is the Boltzmann constant, and $\hbar$ is the Planck constant.

Besides the intensity change, the thermal heating also induces lattice expansion, due to the anharmonicity of the inter-atomic potential. The change of the interatomic distance, *d*, is given by:

$$\Delta d/d_0 = \int_{T_0}^{T_0+\Delta T} \alpha(T) dT \quad (5)$$

where $\alpha(T)$ is the linear expansion coefficient.

S.3 *Ab initio* calculations

Ab initio calculations were performed within the framework of the density functional theory (DFT) and the local density approximation (LDA) using the ABINIT code.[11] We adopted a LDA exchange-correlation functional in the Teter Pade parametrization,[12] and a norm-conserving

Troullier-Martins pseudopotential.[13] Since we are mainly interested in the intra-wall bond length change, we performed the calculations for a single wall armchair nanotube.

The tube unit cell is embedded in a 18.521×18.521×2.494 $Å^3$ super-cell, which is sufficient to avoid any interaction of the tube with its images. An energy cutoff of 20 Ha (544.2 eV) was used for the plane-wave expansion of the electron wave-function. The calculations were carried out fully self-consistently with sixteen *k* points along the tube axis, chosen according to the Monkhorst-Park scheme[14] for the sampling of the Brillouin zone.

The electronic structure is calculated using 68 bands, and the electron excitation in the antibonding states is simulated by modifying the electron occupation of the lowest occupied and the highest unoccupied energy bands. For each band occupation, full structural optimization of the cell geometry was carried out with the Broyden-Fletcher-Goldfarb-Shanno (BFGS) minimization in order to obtain the change of the C-C bond length as a function of the π^* population. Good convergence was obtained with these parameters: a total energy difference smaller than 1.0×10^{-5} eV/atom and Hellman-Feymann forces smaller than 5.0×10^{-3} eV/Å were reached.

In Figure S5 we present the electron density maps calculated for two C-C bonds with a π^* occupation of $1e^-$ as referenced to the ground state ($0e^-$). Their inspection reveals an increase of the electronic charge at the atomic sites, while a corresponding depletion in the region between the carbon atoms takes place, responsible for the C-C bond length increase and thus the observed axial expansion.

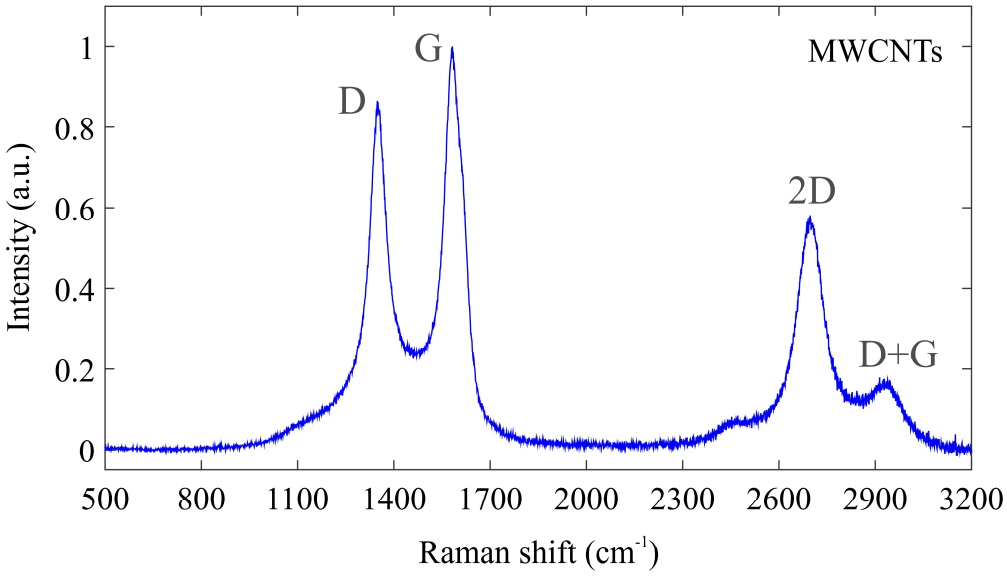

Figure S1. Raman spectrum of the multi-walled carbon nanotubes studied here. The D, G, 2D and D+G bands are labeled. The spectrum is normalized to the G peak (see text).

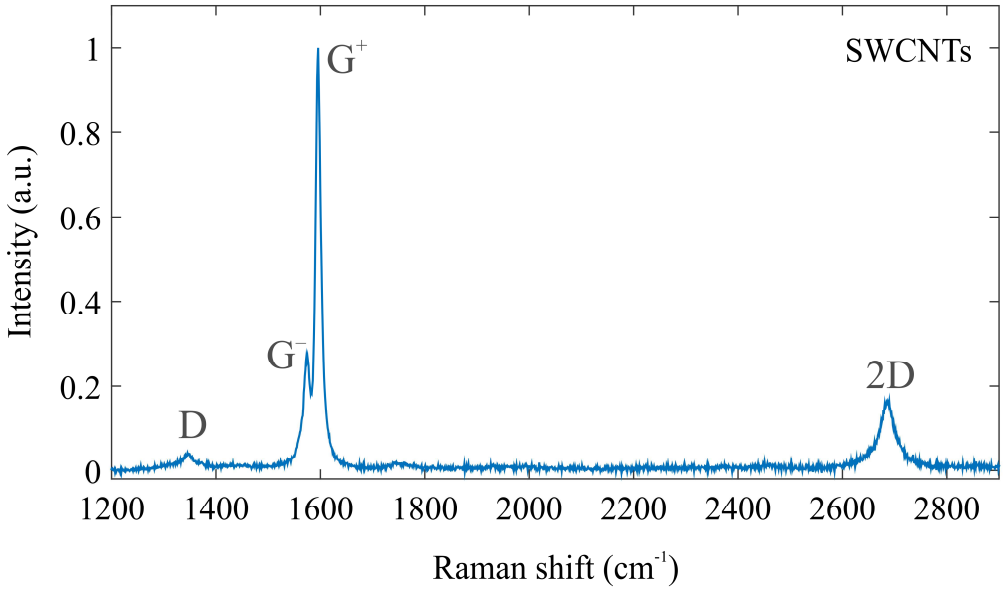

Figure S2. Raman spectrum of the "single-walled" carbon nanotubes studied here. The D, G^+, G^- and 2D bands are labeled. The spectrum is normalized to the G^+ peak (see text).

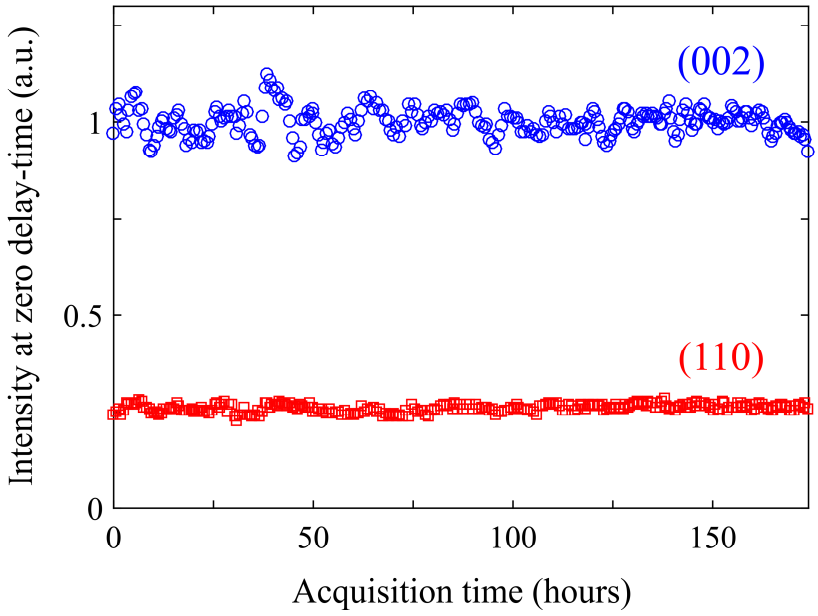

Figure S3. Diffraction intensity vs Acquisition time. The intensity of the (002) and (110) diffraction peaks at zero time-delay is plotted as a function of the acquisition time during the measurements. All data are normalized to the average intensity of the (002) reflection.

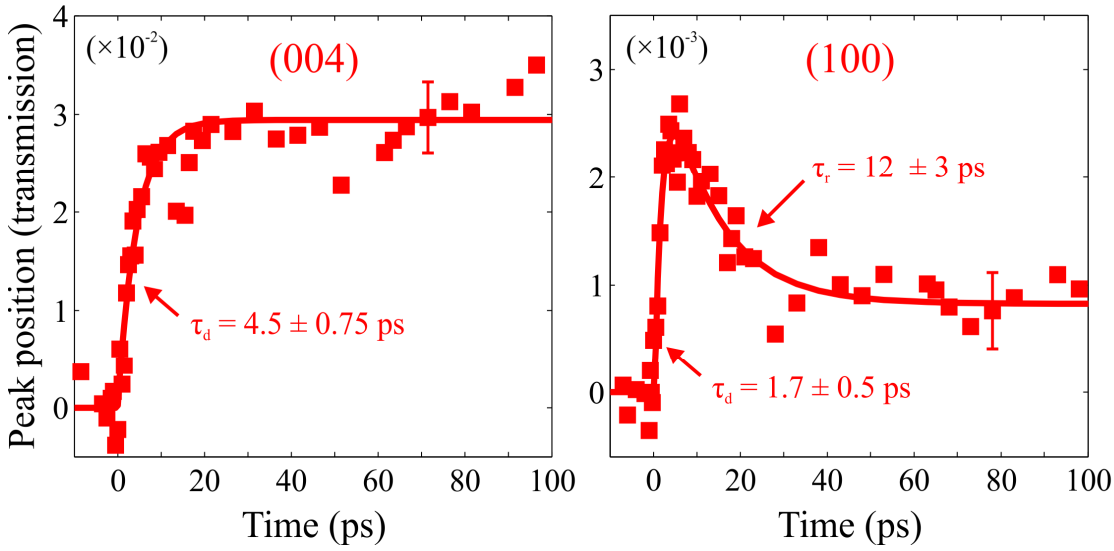

Figure S4. Diffraction (004) and (100) peak-position dynamics. Transient evolution of the peak position (red squares) change for the radial (004) (left) and axial (110) (right) reflections at 48 mJ/cm^2.

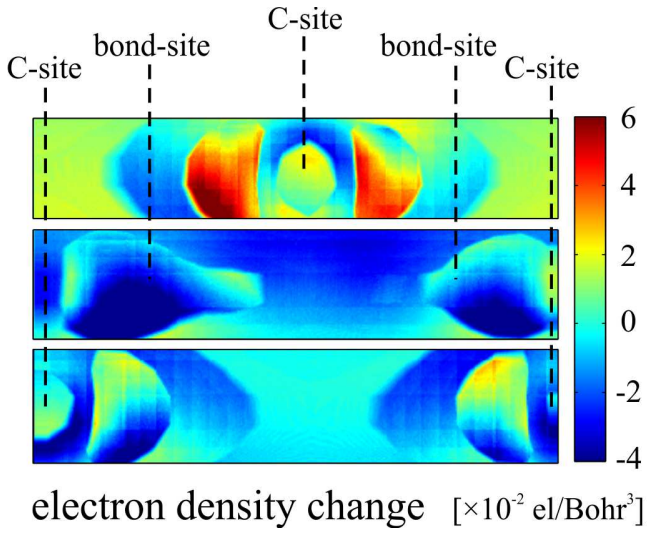

Figure S5. ***Ab initio*** **calculations.** Two-dimensional electron density maps calculated for two C-C bonds oriented along the tube axis with a π^* occupation of $1e^-$ as referenced to the ground state ($0e^-$).

REFERENCES

(1) Dresselhaus, M. S.; Dresselhaus, G.; Saito, R.; Jorio, A. Raman Spectroscopy of Carbon Nanotubes. *Phys. Rep.* **2005**, 409, 47-99.

(2) Lahiri, I.; Lahiri, D.; Jin, S.; Agarwal, A.; Choi, W. Carbon Nanotubes: How Strong Is Their Bond with the Substrate? *ACS Nano* **2011**, 2 780-787.

(3) Gozzi, D.; Latini, A.; Tomellini, M. Thermodynamics of CVD Synthesis of Multiwalled Carbon Nanotubes: A Case Study. *J. Phys. Chem. C* **2009**, 113, 45-53.

(4) Lee, H. S.; Yun, C. H.; Kim, H. M.; Lee, C. J. Persistence Length of Multiwalled Carbon Nanotubes with Static Bending. *J. Phys. Chem. C* **2007**, 111, 18882-18887.

(5) Harris, J. D.; Raffaelle, R. P.; Gennett, T.; Landi, B. J.; Hepp, A. F. Growth of Multi-walled Carbon Nanotubes by Injection CVD Using Cyclopentadienyliron Dicarbonyl Dimer and Cyclooctatetraene Iron Tricarbonyl. *Mat. Sci. Eng. B* **2005**, 116, 369–374.

(6) Piscanec, S.; Lazzeri, M.; Robertson, J.; Ferrari, A. C.; Mauri, F. Optical Phonons in Carbon Nanotubes: Kohn Anomalies, Peierls Distortions, and Dynamic Effects. *Phys. Rev. B* **2007**, 75, 035427.

(7) Schäfer, S.; Liang, W.; Zewail, A. H. Primary Structural Dynamics in Graphite. *New J. Phys.* **2011**, 13, 063030.

(8) Butland, A.; Madison, R. The Specific Heat of Graphite: An Evaluation of Measurements. *J. Nucl. Mater.* **1973**, 49, 45-56.

(9) Pan, H.; Feng, Y.; Lin, J. Ab Initio Study of Electronic and Optical Properties of Multiwall Carbon Nanotube Structures Made Up of a Single Rolled-Up Graphite Sheet. *Phys. Rev. B* **2005**, 72, 085415.

(10) Hauser, J. J. Electrical, structural and optical properties of amorphous carbon. *J. Non-Cryst. Solids* **1977**, 23, 21.

(11) Gonze, X.; Amadon, B.; Anglade, P.-M.; Beuken, J.-M.; Bottin, F.; Boulanger, P.; Bruneval, F.; Caliste, D.; Caracas, R.; Côté, M.; *et al*. ABINIT: First-Principles Approach to Material and Nanosystem Properties. *Computer Phys. Comm.* **2009**, 180, 2582-2615.

(12) Goedecker, S.; Teter, M.; Hutter, J. Separable Dual-Space Gaussian Pseudopotentials. *Phys. Rev. B* **1996**, 54, 1703-1710.

(13) Troullier, N.; Martins, J. L. Efficient Pseudopotentials for Plane-Wave Calculations. *Phys. Rev. B* **1991**, 43, 1993-2006.

(14) Monkhorst, H.J.; Pack, J.D. Special Points for Brillouin-Zone Integrations. *Phys. Rev. B* **1976**, 13, 5188-5192.